5660 *Macromolecules* **2009**, *42*, 5660–5669
DOI: 10.1021/ma802512c

Macromolecules
ARTICLE

UCST-Type Phase Separation and Crystallization Behavior in Poly(vinylidene fluoride)/Poly(methyl methacrylate) Blends under an External Electric Field

Jong Soon Lee,[†] Arun Anand Prabu,[‡] and Kap Jin Kim*

Department of Advanced Polymer & Fiber Materials, School of Chemical and Materials Engineering, College of Engineering, Kyung Hee University, Yongin-si, Gyeonggi-do 446-701, South Korea. [†]*Present address: Analytical Research Center, Hyosung R&DB Laboratories, Anyang-si, Gyeonggi-do 431-080, South Korea.* [‡]*Present address: Department of Chemistry, School of Science & Humanities, Vellore Institute of Technology University, Vellore 632014, Tamil Nadu State, India.*

Received November 10, 2008; Revised Manuscript Received June 21, 2009

ABSTRACT: The effects of an electric field on upper critical solution temperature (UCST) phase separation and crystallization behavior in binary blends of poly(vinylidene fluoride) (PVDF) and poly(methyl methacrylate) (PMMA) were investigated by means of time-resolved small-angle light scattering (SALS) and polarizing optical microscopy (POM). The lower critical solution temperature (LCST) phase separation curve of this blend could not be measured experimentally due to thermal decomposition caused by too high LCSTs. However, the UCST-type phase separation curve was observed from SALS measurements to shift toward higher temperatures under the electric field. In the temperature range above the UCST (150 °C ≤ T ≤ 158 °C), the electric field reduces the overall crystallization rate in the neat PVDF and, in contrast, increases the crystallization rate in 95/5, 90/10, and 85/15 PVDF/PMMA blends. In the temperature range below the UCST (130 °C ≤ T ≤ 143 °C), the electric field also increased the overall crystallization rate in the 80/20 and 70/30 PVDF/PMMA blends. POM images were also used to investigate the effect of the electric field on the overall melt-crystallization rate, nucleation rate, and crystalline morphology in PVDF/PMMA blends.

I. Introduction

Binary polymer blends exhibiting a wide variety of phase morphologies, phase separation characteristics, and dissolution kinetics have been a subject of continuing interest for researchers in both academia and industry due to their widespread applications. Though remarkable progress has been made toward understanding the kinetic aspects of phase separation and dissolution in amorphous−amorphous polymer blends,[1−7] only a few reports have examined crystalline−amorphous polymer blends.[8−14] Among them, poly(vinylidene fluoride)/poly(methyl methacrylate) (PVDF/PMMA) blends have been the most extensively studied because of the rich variety of crystalline morphologies exhibited by PVDF and its ability to form miscible blends with PMMA.[8,9,12,13] PVDF/PMMA blends also exhibit a combination of advantageous physical properties from each individual polymer: the chemical and flame resistance, toughness and piezoelectric characteristics of PVDF, and the tensile strength, low smoke toxicity, and optical properties of PMMA. Such studies are of practical importance for designing polymer blends that incorporate properties that are necessary for commercial applications.

Earlier reports have suggested that the intermolecular interactions in PVDF/PMMA blends are responsible for the lower critical solution temperature (LCST, around 350 °C) behavior at temperatures well above the melting temperature (T_m) of PVDF (ca. 178 °C).[9,12] According to Walker et al., the pendant carbonyl sites in PMMA that are capable of forming hydrogen bonds or exerting dipole−dipole interactions with the CH_2 or CF_2 groups of PVDF are responsible for the complete miscibility of PVDF/PMMA blends observed over a wide range of temperatures in the melt state.[12] On the other hand, PVDF/PMMA blends have also been reported to exhibit partial miscibility at temperatures below their T_m and exist in the amorphous state over a broad range of compositions (up to 50 wt % of PVDF).[12] In another study, Tomura et al. reported the occurrence of liquid−liquid phase separation, also known as upper critical solution temperature (UCST)-type phase behavior at temperatures far below their T_m.[9] Thus, crystallization takes place above the UCST, and liquid−liquid phase separation occurs below the UCST.

Since PVDF is electroactive, it is logical to investigate the effect of applying an external electric field on the phase decomposition behavior and on the melt-crystallization behavior above and below the UCST in PVDF blends. However, only a few reports are available that discuss the phase diagrams and phase separation behavior of polymer solutions and polymer−polymer blends under an electric field, including a recent study from our research group.[15−20] A detailed literature survey indicates that no previous studies have reported the phase diagram and phase separation behavior of PVDF/PMMA blends under an electric field. In the present study, the effect of an external electric field on the phase separation and crystallization behavior of PVDF/PMMA blends above and below the UCST were examined on the basis of a new theoretical equation along with experimental studies, and the results are discussed in detail.

II. Experimental Section

Materials and Sample Preparation. Polydisperse PVDF resin (Kynar 761, M_w = 480 000, Atofina Co.) and polydisperse

*Corresponding author: Ph +82-31-201-2518; Fax +82-31-204-8114; e-mail kjkim@khu.ac.kr.

 Published on Web 07/10/2009

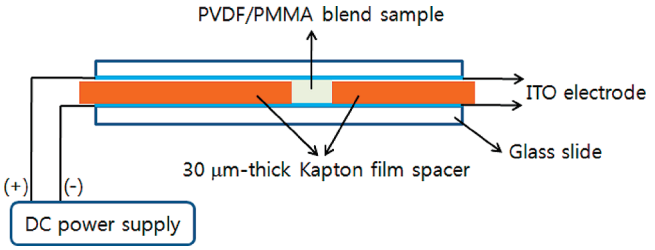

Figure 1. Schematic diagram of experimental setup adopted to apply a dc voltage to the PVDF/PMMA blend for time-resolved 2-D small-angle light scattering measurement and microscopic observation under an external electric field.

PMMA (M_w = 350 000, Sigma-Aldrich) were used as received. PVDF and PMMA were dissolved separately in *N,N*-dimethylformamide (DMF) used as cosolvent. Each of 4 wt % stock solutions was subsequently mixed with varying PVDF/PMMA composition ratios followed by precipitation of the polymer blend in copious amounts of deionized water. The precipitate was washed many times with deionized water to remove the residual solvent, and the products were dried in a vacuum oven for 5 days at 85 °C. About 50 μm thick films of each PVDF blend composition were prepared by melt-pressing the powdered samples using a Carver press, and the films were quenched in iced water. The dried blend films were placed between two glass slides having a transparent ITO conducting layer in their inner surfaces using a 30 μm thick Kapton film spacer. As shown in Figure 1, the spacer has a squared hole (5 × 5 mm^2) in the center of the film to prevent potential electrical shortage caused by air under an external electric field (0−7 MV/m).

Time-Resolved 2-D Small-Angle Light Scattering (SALS) Measurement under an External Electric Field. The apparatus used for the time-resolved 2-D SALS measurements under an external electric field was similar to that used in our previous study.[20] For temperature-quench (T-quench) experiment under an external electric field, the sample was maintained at a single phase temperature of 220 °C for 15 min under an external electric field of required field strength. Then the sample was rapidly transferred to the hot stage on the light scattering apparatus, which was kept at the desired temperature below the T_m. The scattering pattern by phase separation and/or crystallization was then recorded and saved in a personal computer as a function of time. Two optical geometries were adopted. One is the H_v geometry for the observation of the crystallization behavior, and the other is the V_v geometry for observation of both crystallization behavior and liquid−liquid phase separation. When the V_v scattering profiles were measured, a neutral density filter (with an optical density of 2) was inserted into the laser light beam path to attenuate the intensity of the incident laser light and to reduce parasitic scattering.

As a double-layered and/or a triple-layered sandwich can be formed in the course of melting the sample, the thickness of the sample placed between the ITO glass slides cannot be the same as the thickness of the Kapton film spacer. Thus, the real sample thickness must be measured to calculate the dc voltage required to apply to the sample with desired electric field strength. We first measured the total thickness of the ITO-coated glass slides containing only the Kapton spacer. After the sample was completely melted at 220 °C, the thickness of the ITO-coated glass slides containing the Kapton spacer and the sample was measured. The distance between the electrodes was calculated as the summation of the Kapton film thickness and the thickness difference between the first and second measurements. The dc high-voltage supplier used was a PMT-75C model manufactured by Bertan Co.

Polarizing Optical Microscopy (POM) under an External Electric Field. Melt-crystallization at isothermal conditions in the presence of an electric field was carried out using a POM (Nikon Optiphot-POL) equipped with a Mettler FP82 hot stage, a photodetector, and a Watec CCD camera. After melting at 220 °C for 15 min under an external electric field (0−5 MV/m), each sample was quenched to the desired isothermal temperature at the maximum cooling rate allowed. The temperature used for T-quench experiments in this study was similar to that used previously in the SALS measurement. Each microscopic image was saved in order to observe and analyze the crystalline morphology. The transmitted light intensity under cross-polarization was also recorded simultaneously as a function of crystallization time in order to evaluate the overall crystallization rate.

DSC Measurement. Thermograms of the PVDF/PMMA blend samples that were previously subjected to melt-crystallization at different isothermal temperatures were measured (at least in duplicate) using a Perkin-Elmer DSC-4 differential scanning calorimeter (DSC) calibrated with the melting temperature of indium. DSC curves of the samples were obtained under a nitrogen atmosphere with a heating rate of 10 °C/min.

III. Theoretical Background

When an electric field is applied to a polymer solution, the Flory−Huggins parameter, χ_c, increases at a critical concentration, ϕ_c, with increasing electric field strength, resulting in a lower UCST and a higher LCST. As an evidence toward this thought, Wirtz et al. suggested and validated this theory by simultaneously studying the phase behavior of polystyrene/cyclohexane mixture and poly(*p*-chlorostyrene)/ethylcarbitol mixture solutions under an electric field via laser light scattering measurements.[16] Using different theoretical equations, Gurovich[17,18] predicted that the UCST in a polymer solution or polymer−polymer blend decreases with increasing electric field strength. However, in our previous report, we experimentally showed the opposite result for the LCST-type phase separation of PVDF/poly(1,4-butylene adipate) (PBA) blends in the presence of an external electric field.[20] The binodal curve fitted with the cloud points obtained experimentally from SALS measurements was shifted toward lower temperature in the presence of the electric field. Consequently, the field-induced phase separation and the field removal-induced phase dissolution could be observed reversibly for the 9/1 and 7/3 blends. The origin of this shift in the LCST toward lower temperature in the presence of the electric field for PVDF/PBA blends was elucidated by adding free energy term that considers the external electric field to the conventional Flory−Huggins equation as shown in eq 1.[20]

$$\Delta G_m(E)/V = RT\left(\frac{\phi_1}{V_1}\ln\phi_1+\frac{\phi_2}{V_2}\ln\phi_2+\chi\phi_1\phi_2\right)-\frac{1}{2}\varepsilon_0\varepsilon E^2 \quad (1)$$

where $\Delta G_m(E)/V$ is the free energy of mixing per unit volume under an electric field, ϕ_1 and ϕ_2 are the volume fractions of polymer A and polymer B, respectively, and V_1 and V_1 are the molar volumes of polymer A and polymer B, respectively, R is the universal gas constant, χ is the Flory−Huggins interaction parameter, ε_0 is the vacuum dielectric constant, ε is the relative dielectric constant of the blend, and E is the external electric field strength.

A linear relationship between the refractive index and volume fraction has been reported for binary solutions by Glover and Goulden[21] as given in the following equation:

$$n = n_1+\frac{(n_2-n_1)V_2}{V_1+V_2} = n_1+(n_2-n_1)\phi_2 \quad (2)$$

where n is the refractive index of the solution, n_1 is the refractive index of the solvent, n_2 is the refractive index of the solute, V_1 is

the volume occupied by the solvent, V_2 is the volume occupied by the solute, and ϕ_2 is the volume fraction of the solute. The application of this linear relationship to a binary polymer mixture yields a constant of $\partial n/\partial\phi_2 = n_2 - n_1$. Assuming that χ is independent of the concentration ϕ_2 and $\varepsilon = n^2$, we can obtain the critical composition ($\phi_{2,c}(E)$) and critical χ parameter ($\chi_c(E)$) after simultaneously satisfying the conditions $\partial^2(\Delta G_m(E))/\partial\phi_2{}^2 = 0$ and $\partial^3(\Delta G_m(E))/\partial\phi_2{}^3 = 0$, as follows:

$$\phi_{2,c}(E) = \frac{\sqrt{V_1}}{\sqrt{V_1}+\sqrt{V_2}} = \phi_{2,c}(0) \tag{3}$$

$$\chi_c(E) - \chi_c(0) \cong -\frac{\varepsilon_0 E^2}{4RT_c(E)}\left(\frac{\partial^2\varepsilon}{\partial\phi_2{}^2}\right)_c \cong -\frac{\varepsilon_0 E^2}{2RT_c(E)}\left(\frac{\partial n}{\partial\phi_2}\right)^2 < 0 \tag{4}$$

$\chi(T)$ can be expressed as shown in eq 5.

$$\chi(T) = a + \frac{b}{T} \tag{5}$$

and the combination of eq 5 with eq 4 yields eqs 6a and 6b.

$$1/T_c(E) - 1/T_c(0) \cong -\frac{\varepsilon_0 E^2}{2bRT_c(E)}\left(\frac{\partial n}{\partial\phi_2}\right)^2 \tag{6a}$$

$$\frac{T_c(E) - T_c(0)}{T_c(0)} \cong \frac{\varepsilon_0 E^2}{2bR}\left(\frac{\partial n}{\partial\phi_2}\right)^2 \tag{6b}$$

Therefore, the critical temperature ($T_c(E)$) increases with electric field for the UCST and the critical temperature ($T_c(E)$) decreases with electric field for the LCST, because a is negative and b is positive for the UCST and a is positive and b is negative for the LCST. The theoretical prediction that the critical temperature decreases with an increase in electric field strength for LCST-type phase decomposition was suggested experimentally by the phase separation behavior of the PVDF/PBA blends in the presence of an external electric field.[20] However, since the PVDF/PBA blends do not show any additional UCST-type phase decomposition below the LCST, we could not verify the predicted effect of an electric field on the UCST-type phase separation behavior in PVDF/PBA blends. In order to obtain a phase diagram including both the LCST and the UCST for PVDF/PMMA blends, an additional term $c \ln T$ is required in eq 5.[22] However, it is very difficult to empirically obtain the LCST curve due to thermal degradation caused by an extremely high critical temperature. Hence, eq 5 in the present form is thought to be sufficient for explaining UCST behavior, while avoiding the calculation complexity that would be caused by adding the $c \ln T$ term. According to Tomura et al.,[9] PVDF/PMMA blends can have a UCST below the melting temperature of PVDF as well as an LCST above 350 °C as drawn schematically in Figure 2, though this is uncommon. However, under an electric field, it is possible to predict a shift in the LCST to a lower temperature and a shift in the UCST to a higher temperature in PVDF/PMMA blends as discussed below.

IV. Results and Discussion

Effect of an Electric Field on the USCT in PVDF/PMMA Blends. Figure 3 shows the H_v and V_v scattering profiles for the 80/20 PVDF/PMMA blend after quenching to 145 °C from a single phase at 220 °C. Both the H_v and the V_v scattering intensities increase with elapsed time. It is well-known that the H_v scattering intensity varies with optical

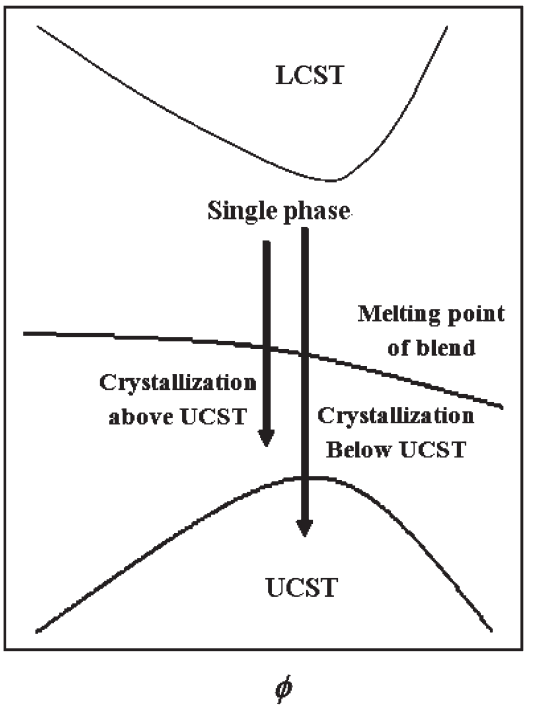

Figure 2. Schematic phase diagram of a PVDF/PMMA blend exhibiting a UCST and an LCST. The LCST of the PVDF/PMMA blend cannot be measured experimentally due to thermal degradation caused by too high LCST. When the PVDF/PMMA blend was crystallized isothermally after cooling down from the melt state (single phase), two crystallization temperature ranges were selected: one above the UCST and one below the UCST.

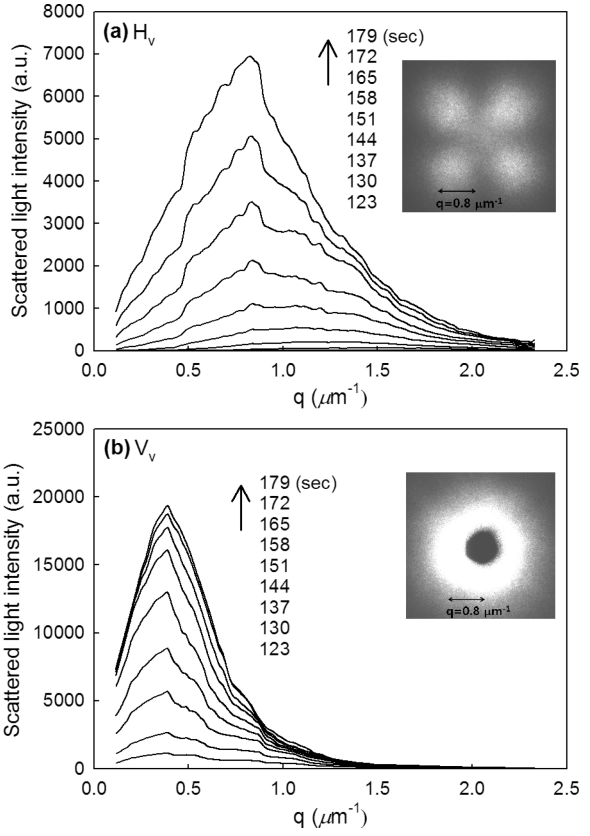

Figure 3. Changes in (a) H_v and (b) V_v laser light scattering profiles with time after quenching from 220 to 145 °C for the 80/20 PVDF/PMMA blend. Inset (a): 2-D H_v pattern; inset (b): 2-D V_v pattern at 151 s.

anisotropic changes caused by changes in crystallinity over the course of melt-crystallization for an unoriented sample or by changes in the degree of orientation during drawing process for a fiber or a film. The V_v scattering intensity varies with both optical anisotropic changes and fluctuations in concentration caused by liquid−liquid phase separation. To investigate the liquid−liquid phase separation behavior in crystalline−amorphous polymer blends in which melt-crystallization and liquid−liquid phase separation occur simultaneously, the V_v scattering light intensities attributed to liquid−liquid phase separation must be separated from the scattering light intensities associated with melt-crystallization. To obtain information regarding the melt-crystallization and liquid−liquid phase separation kinetics, it is common to use the integrated scattering intensity, i.e., the invariant Q as defined by eq 7.

$$Q = \int_0^\infty I(q) q^2 \, dq \tag{7}$$

where the scattering vector $q = (4\pi/\lambda)\sin(\theta/2)$, in which λ and θ are the wavelength of the incident light and the scattering angle in the sample, respectively. $I(q)$ is the intensity of the scattered light at q.

Since the crystals that formed in the PVDF/PMMA blends during crystallization were spherulitic, the H_v scattering pattern was a four-leaf clover type. $I(q)_{H_v}$ was obtained by scanning along the radial direction of one-leaf clover type scattering pattern, and $I(q)_{V_v}$ was obtained by scanning along the same radial direction used in $I(q)_{H_v}$ scanning. The invariant in the H_v mode, Q_{H_v}, is related to the mean-square optical anisotropy $\langle \delta^2 \rangle$, as shown in eq 8.

$$\langle \boldsymbol{\delta}^2 \rangle \propto \phi_s (\alpha_r - \alpha_t)^2 \tag{8}$$

where ϕ_s is the volume crystallinity, i.e., the fraction of spherulites, and α_r and α_t are the radial and tangential polarizabilities of spherulites, respectively. Therefore, Q_{H_v} increases with increasing crystallinity. On the other hand, the invariant in the V_v mode, Q_{V_v}, is related to both $\langle \delta^2 \rangle$ and the mean-square concentration fluctuation $\langle \eta^2 \rangle$. The term $\langle \eta^2 \rangle$ refers to the mean-square average of all polarizability fluctuations for light scattering of a two-phase mixture as expressed in eq 9.[23]

$$\langle \eta^2 \rangle \propto \phi_1 \phi_2 (\alpha_1 - \alpha_2)^2 \propto \phi_1 (1 - \phi_1)(\alpha_1 - \alpha_2)^2 \tag{9}$$

where ϕ_1 and ϕ_2 are the volume fractions, and α_1 and α_2 are the polarizabilities of the two phases, respectively.

Thus, $\langle \eta^2 \rangle$ in a pure crystalline polymer system is defined as eq 10.

$$\langle \eta^2 \rangle \propto \phi_s (1 - \phi_s)(\alpha_c - \alpha_a)^2 \tag{10}$$

where α_c is the average polarizability of the spherulites and α_a is the polarizability of the amorphous phase. In a phase-separated blend of polymers A and B with a sharp phase boundary, $\langle \eta^2 \rangle$ is similarly described by eq 11.

$$\langle \eta^2 \rangle \propto \phi_A (1 - \phi_A)(\alpha_A - \alpha_B)^2 \tag{11}$$

where ϕ_A is the volume fraction of the A-rich phase and α_i is the polarizability of the i-rich phase.

Figure 4 shows the time variations of the invariants Q_{H_v} and Q_{V_v} calculated from the scattering intensity data in Figure 3. As seen in Figure 4, both invariants increase with annealing time after remaining unchanged for a certain period of time. The invariant Q_{V_v} can be found to increase before Q_{H_v}. This indicates that, initially, the phase separation occurs slightly before melt-crystallization, and at a later stage, both the phase separation and crystallization occur simultaneously. The initial slope of the Q_{H_v} time variation (Q_{H_v}/dt) represents the relative rate of crystallization, whereas dQ_{V_v}/dt represents the crystallization rate and the liquid−liquid phase separation rate. In the phase separation of crystalline−amorphous binary mixtures showing UCST behavior below the melting temperature of the crystalline polymer, crystallization and liquid−liquid phase separation occur simultaneously. Hence, a pure liquid−liquid phase separation cannot be estimated using only Q_{V_v} due to the additional contributions of crystallization and liquid−liquid phase separation to the light scattering intensity in V_v mode. Therefore, one must subtract the contribution of crystallization from the resultant Q_{V_v} using Q_{H_v} which only has the crystallization contribution. However, this subtraction method is not completely accurate quantitative-wise. There are significantly different scattering patterns in H_v and V_v modes for spherulitic crystals. Additionally, there is a vital difference in the incident beam intensity caused by the use of a neutral filter in the V_v mode in order to reduce the laser beam significantly to protect the CCD camera and to adjust the maximum scattering intensity below the full well capacity of CCD pixel. Therefore, instead of using the subtraction method, a ratio of the two rates, $\kappa = (dQ_{V_v}/dt)/(dQ_{H_v}/dt)$, can be assumed to describe the relative rate of the liquid−liquid phase separation.[9]

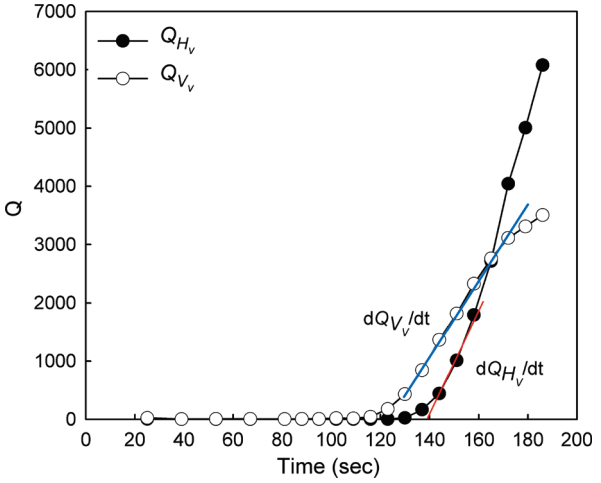

Figure 4. Time variation of the invariants Q_{H_v} and Q_{V_v} for the 80/20 PVDF/PMMA blend after quenching from 220 to 145 °C.

Figure 5 shows plots of κ versus quenching temperature for neat PVDF and various PVDF/PMMA blends. Since there is no phase separation in the case of neat PVDF (Figure 5a), the invariants Q_{V_v} and Q_{H_v} are purely associated with crystallization of PVDF, and the κ value seems to be nearly constant with respect to the temperature. However, the values of the PVDF/PMMA blends depend on their quench temperature (T_q). As T_q decreases, the κ value initially remains nearly constant and then abruptly increases at a transition temperature (T_{tr}) and identified as a UCST-based phase separation temperature. This suggests that the UCST-type liquid−liquid phase separation starts to occur when $T_q < T_{tr}$. In other words, the contribution of the melt-crystallization to the overall scattered light

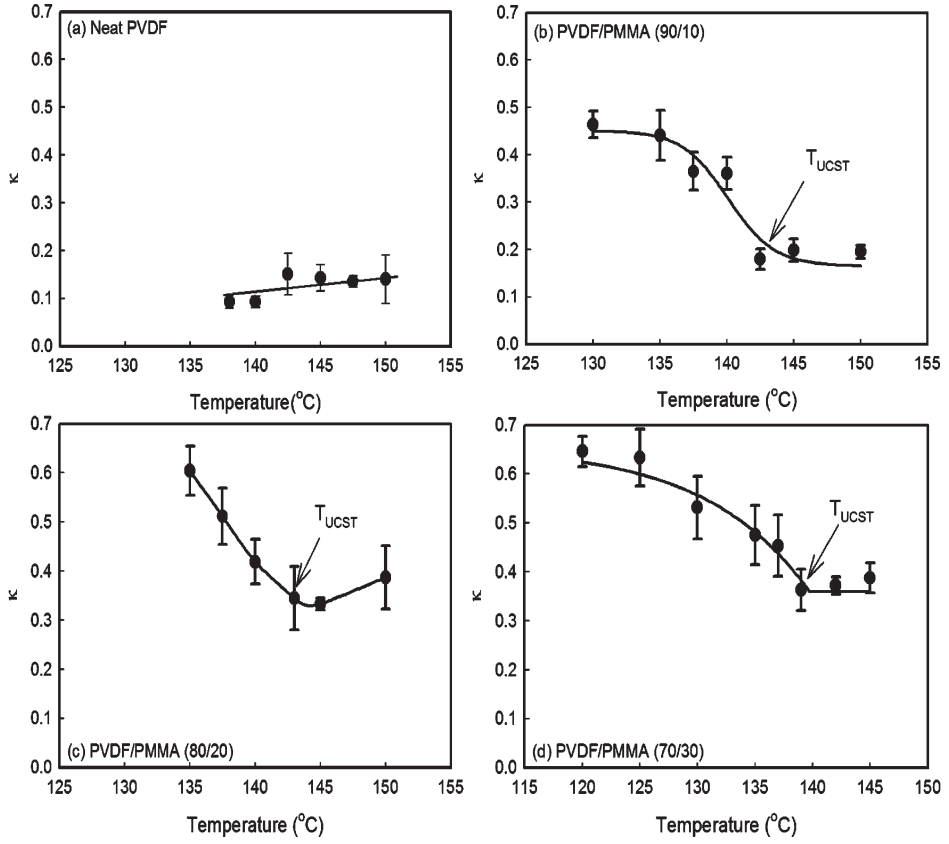

Figure 5. Temperature dependence of κ in the absence of an electric field: (a) neat PVDF, (b) PVDF/PMMA (90/10), (c) PVDF/PMMA (80/20), and (d) PVDF/PMMA (70/30).

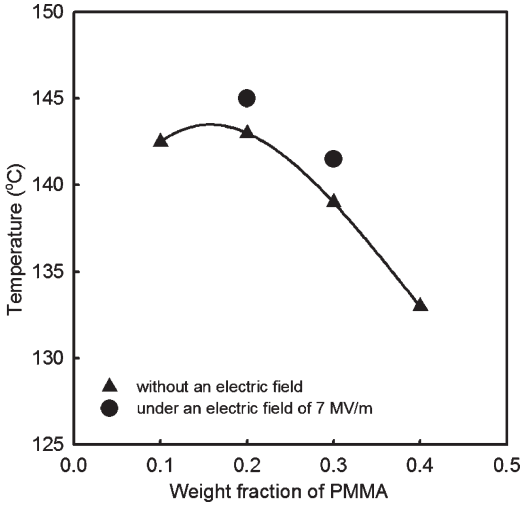

Figure 6. UCST-type binodal points versus PMMA content for the PVDF/PMMA blends with and without an electric field of 7 MV/m. The curve is drawn to guide the eyes.

intensity $I(q)_V$ is assumed to be negligible at early stages when $T_q < T_{tr}$. Thus, T_{tr} can be considered to be a pseudobinodal point. For the 90/10, 80/20, 70/30, and 60/40 PVDF/PMMA blends, T_{tr} was observed at around 142.5, 143, 138, and 133 °C (not shown in the figure), respectively. The new UCST-type binodal points of the PVDF/PMMA blends in the absence of an electric field are plotted as closed triangles in Figure 6. Binodal points in the presence of an electric field were obtained similarly and are plotted in Figure 6 as closed circles. The binodal points obtained under an electric field of 7 MV/m were slightly higher than those obtained in the absence of an electric field by 2−2.5 °C. Unfortunately, we could not obtain reproducible T_{tr} values for the 90/10 and 60/40 blends under an electric field of 7 MV/m. Under an electric field of less than 5 MV/cm, we could not obtain consistent results because increases in the UCST were negligible. Moreover, with an electric field greater than 10 MV/m, consistent results were not obtained due to frequent electrical shortages caused by the increased current. In our previous work, we reported a decrease of LCST-type binodal points for PVDF/PBA blends under the electric field.[20] Considering these results, we can conclude that the electric fields thermodynamically destabilize PVDF/PMMA blends. Consequently, the LCST can be lowered and the UCST can be increased, if empirically possible.

Effect of an Electric Field on the Crystalline Morphology and Melt-Crystallization Behavior of PVDF/PMMA Blends above the UCST. Figure 7 shows the microphotographs of the 85/15 PVDF/PMMA blends during isothermal melt-crystallization at 158 °C with and without an electric field (5 MV/m). The microphotographs were recorded with a polarizing microscope under cross-polarization as a function of crystallization time. The number and volume fraction of spherulites were much higher under an electric field than when $E_0 = 0$ for the same crystallization time. From this result, we can expect that the rate of overall melt-crystallization and the rate of nucleation under an electric field are greater than without an electric field for the PVDF/PMMA blends.

The rate of overall crystallization can be estimated with the reciprocal of the half-crystallization time $((t_{1/2})^{-1})$ obtained from the transmitted depolarized light intensity

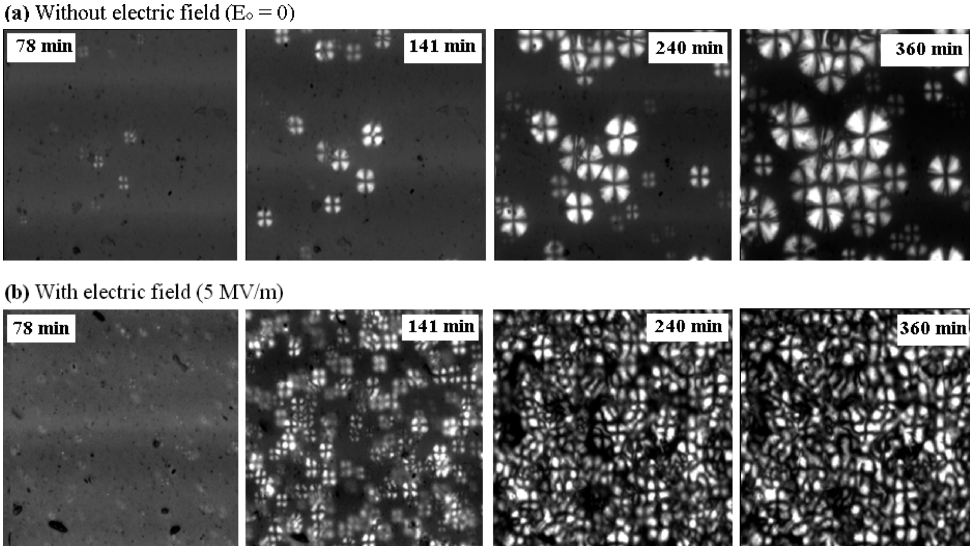

Figure 7. Microphotographs as a function of crystallization time: (a) in the absence of electric field and (b) in the presence of an electric field (5 MV/m) at 158 °C for the 85/15 PVDF/PMMA blend.

data acquired as a function of time under cross-polarization. Figure 8 shows plots of $(t_{1/2})^{-1}$ versus crystallization temperature with and without an electric field for PVDF and PVDF/PMMA blends. In the temperature range between 150 and 158 °C (in Figure 8) where nonpolar α-crystals are dominantly formed, the electric field reduces the overall crystallization rate in a pure PVDF as reported in the literature,[25−27] while increasing the rate in PVDF/PMMA blends.

Marand's theoretical equation that describes the primary nucleation rate (I_e^*) with an electric field as a function of field strength[25] was modified in the present study, and a new equation was derived for the spherulitic growth rate (G_e^*) under an electric field.[27]

$$\log(I_e^*/I_0^*) = \frac{32\sigma^2\sigma_e}{2.303kT}\left\{\left(\frac{1}{\Delta h\Delta T/T_m^0}\right)^2 - \left(\frac{1}{\Delta h\Delta T/T_m^0 + PE_0}\right)^2\right\} \quad (12)$$

and

$$\log(G_e^*/G_0^*) = \frac{4b_0 i\sigma\sigma_e}{2.303kT}\left(\frac{1}{\Delta h\Delta T/T_m^0} - \frac{1}{\Delta h\Delta T/T_m^0 + PE_0}\right) \quad (13)$$

where I_0^* is the primary nucleation rate without electric field, G_0^* is the spherulitic growth rate without electric field, σ is the side-surface free energy of the nucleus, σ_e is the end-surface free energy of the nucleus, b_0 is the thickness of a monomolecular layer in the (110) plane of PVDF, i is the regime kinetic constant, Δh is the heat of fusion per unit volume of the crystal, k is Boltzmann's constant, T_m^0 is the equilibrium melting temperature, T is the crystallization temperature, ΔT is the undercooling ($T_m^0 - T$), E_0 is the field strength, and P is the polarization per unit volume of the crystal. P is represented as the permanent polarization, P_p (eq 14), for polar γ-crystals, whereas P is represented as the induced polarization, P_i, for nonpolar α-crystals (see eq 15).[25]

$$P_p = \frac{2\varepsilon_a}{\varepsilon_a + \varepsilon_c}P_c \quad (14)$$

and

$$P_i = \varepsilon_0\varepsilon_a\frac{\varepsilon_c - \varepsilon_a}{\varepsilon_c + \varepsilon_a}E_0 \quad (15)$$

where P_c is the vacuum polarization of the polar crystal, ε_0 is the vacuum dielectric constant, ε_c is the relative dielectric constant of the polar crystal, and ε_a is the relative dielectric constant of the amorphous phase.

Polar γ-crystals always have a positive value of P_p, whereas nonpolar α-crystals have a negative value of P_i because $\varepsilon_c < \varepsilon_a$. Thus, for a given undercooling, the ratios I_e^*/I_0^* and G_e^*/G_0^* increase with field strength for a polar phase, such as a γ-crystal. Consequently, the overall crystallization rate increases with field strength. In contrast, the above ratios decrease with increasing field strength for a nonpolar phase such as α-crystalline phase. Consequently, the overall crystallization rate decreases with field strength. This qualitative analysis helps to explain why the overall rate of crystallization decreases with increasing field strength for the melt-crystallization of neat PVDF. This analysis, however, cannot explain why the number of spherulites and the overall crystallization rate increase with increasing field strength for the melt-crystallization of PVDF/PMMA blends. If eqs 14 and 15 which were used for pure PVDF are also applied to the analysis of the melt-crystallization behavior of PVDF/PMMA blends under the electric field, the condition of $\varepsilon_c > \varepsilon_a$ can only explain why the nucleation and overall crystallization rates increase with the field strength. However, the origin of $\varepsilon_c > \varepsilon_a$ cannot be explained at present for the PVDF/PMMA blend.

Figure 9 shows the melting endotherms of neat PVDF melt-crystallized isothermally at various temperatures (scan rate = 10 °C/min) with and without an electric field of 5 MV/m. The minor shoulder endothermic peak in the range of 160−167 °C originated from the melting of thermodynamically unstable α-crystal initially formed, and the main melting peak observed in the range of 169−172 °C is assigned to

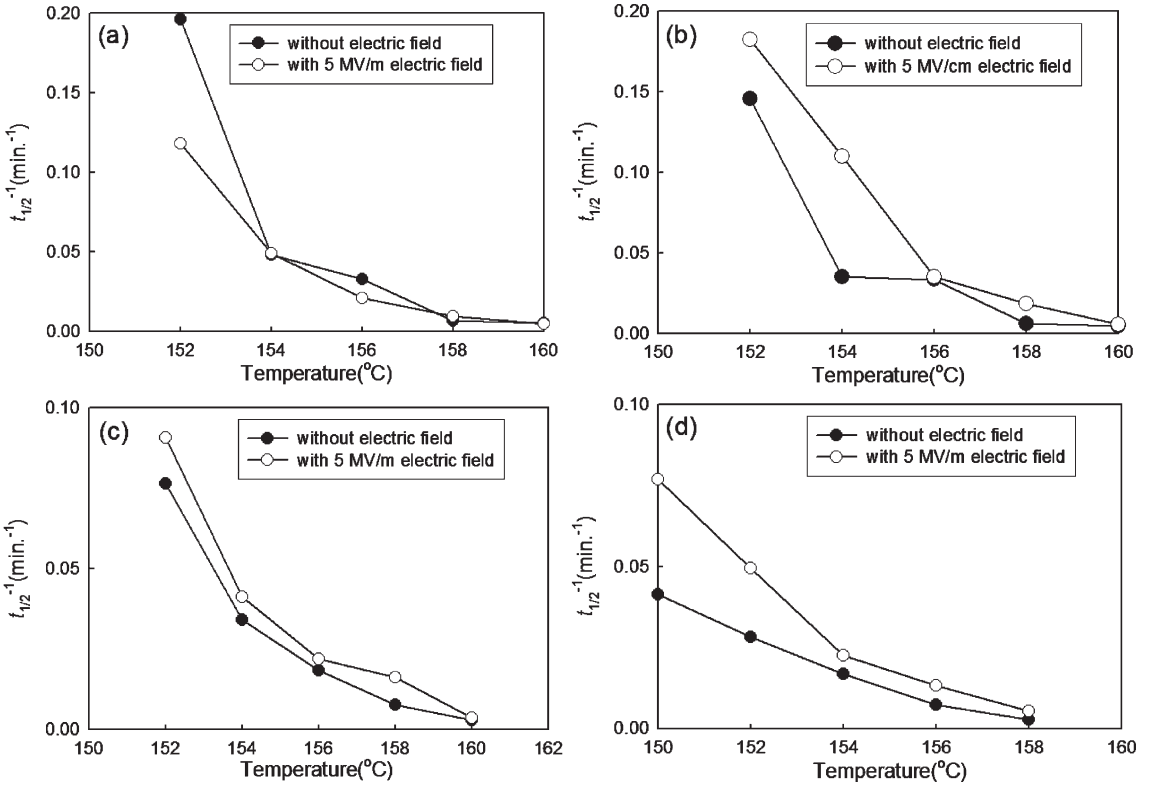

Figure 8. Plots of $t_{1/2}^{-1}$ versus crystallization temperature for PVDF and PVDF/PMMA blends crystallized at various temperatures above the UCST with and without an electric field: (a) PVDF, (b) PVDF/PMMA (95/5), (c) PVDF/PMMA (90/10), and (d) PVDF/PMMA (85/15).

the melting of thermodynamically stable α-crystal.[24] The shoulder peak temperature in the range of 160−167 °C is dependent on crystallization temperature. This shoulder peak is observed to shift from initial 160 to 167 °C due to increasing stability of the initially formed α-crystal with the crystallization temperature changing from 152 to 160 °C. The small endothermic peak observed in the range of 177−180 °C is assigned to the γ-crystal formed during melt-crystallization, and the small endothermic peak that appears in the range of 186−189 °C is assigned to the melting of the γ′-crystal, which was transformed from an α-crystal during isothermal melt-crystallization.[25] It is observed that the melting point decreases with increasing PMMA content. This melting point depression is due to the excellent attraction between PVDF and PMMA caused by dipole−dipole interactions. The interaction energy density (B) and the Flory−Huggins interaction parameter (χ) between PVDF and PMMA can be obtained from this melting point depression data; however, this is not reported here since it is sufficiently discussed in the literature.[8,9,12]

Table 1 presents the crystalline morphology map obtained from POM and DSC results of the PVDF/PMMA blends crystallized from the melt with and without an external electric field. For the 90/10 and 85/15 PVDF/PMMA blends, ring-banded spherulites were observed at higher crystallization temperatures under an electric field, as reported for the PVDF/poly(vinyl acetate)[28] and PVDF/poly(ethylene-*co*-vinyl acetate)[29,30] blends crystallized without an electric field. γ-Crystals were observed at a lower crystallization temperature under an electric field than in the absence of an electric field. However, the reason why the electric field preferentially formed ring-banded spherulites and γ-crystals was not identified. The transformation of α-crystals to

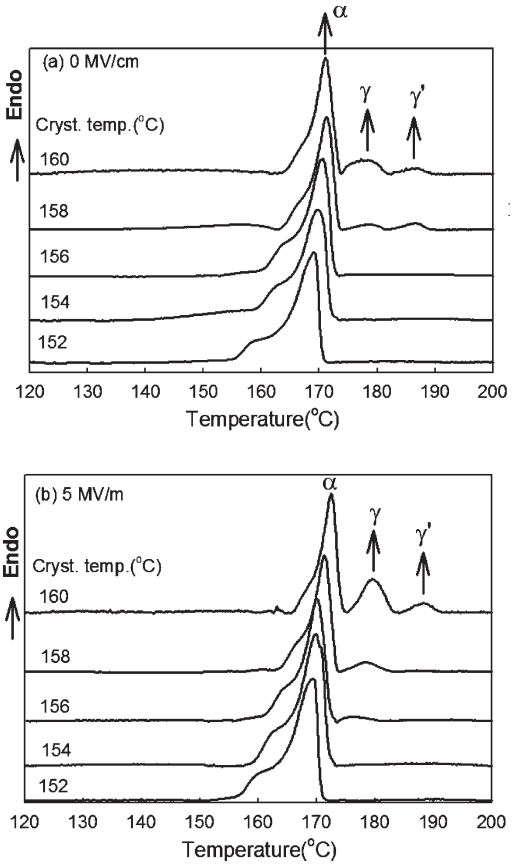

Figure 9. Melting endotherms of PVDF melt-crystallized isothermally at various temperatures: (a) without electric field and (b) under an electric field (5 MV/m). Scan rate = 10 °C/min.

Table 1. Crystal Morphology Map of PVDF/PMMA Blends Crystallized from the Melt with and without an External Electric Field[a]

	PVDF		PVDF/PMMA (95/5)		PVDF/PMMA (90/10)		PVDF/PMMA (85/15)	
temp (°C)	0	5 MV/m	0	5 MV/m	0	5 MV/m	0	5 MV/m
150							L_α	L_α
152	L_α	L_α			L_α	L_α	L_α	L_α
154	L_α	L_α	L_α	L_α	L_α	L_α/L_γ	L_α	L_α/L_γ
156	L_α	L_α/L_γ	L_α	L_α	L_α/L	$L_\alpha/C/L_\gamma$	$L_\alpha/L_\gamma/L_{\gamma'}$	$L_\alpha/C/L_\gamma/L_{\gamma'}$
158	L_α/L_γ	L_α/L_γ	L_α	L_α/L_γ	$L_\alpha/L_\gamma/L_{\gamma'}$	$L_\alpha/C/L_\gamma$	$L_\alpha/L_\gamma/L_{\gamma'}$	$L_\alpha/C/L_\gamma/L_{\gamma'}$
160	$L_\alpha/L_\gamma/L_{\gamma'}$	$L_\alpha/L_\gamma/L_{\gamma'}$	L_α/L_γ	L_α/L_γ		$L_\alpha/C/L_\gamma/L_{\gamma'}$		
162			$L_\alpha/L_\gamma/L_{\gamma'}$	$L_\alpha/L_\gamma/L_{\gamma'}$				

[a] L: lamellar splay type spherulite; C: concentric ring banded spherulite; α: alpha-crystal phase; γ: gamma-crystal phase originally formed; γ′: gamma-crystal phase formed through the crystalline transition of α-crystal phase.

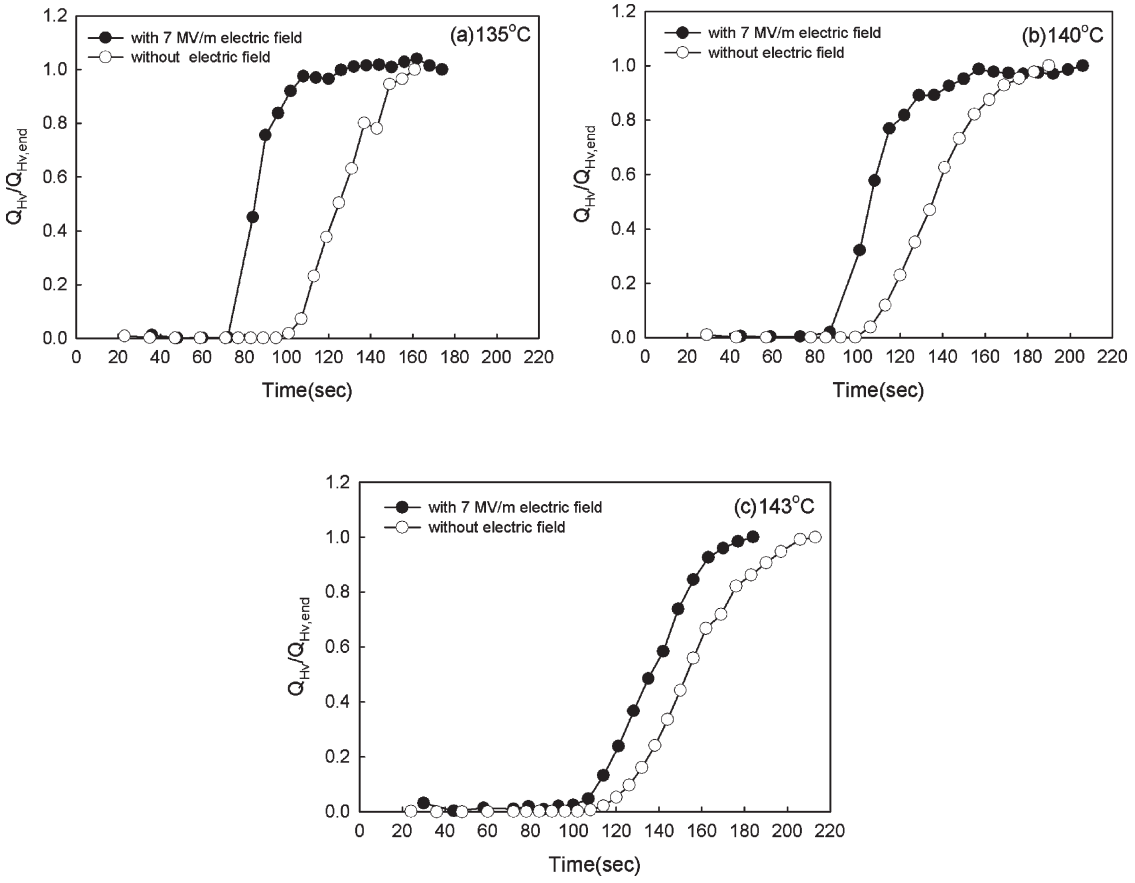

Figure 10. Normalized degree of crystallization versus time for the 80/20 PVDF/PMMA blend with and without an electric field of 7 MV/m after quenching from 220 °C to (a) 135 °C, (b) 140 °C, and (c) 143 °C below the UCST.

γ′-crystals was observed with increasing PMMA content and at higher crystallization temperatures; however, the effect of an electric field was not determined.

Effect of an Electric Field on the Crystallization Behavior of PVDF/PMMA Blends below the USCT. When the PVDF/PMMA blends were quenched from a single phase state (at 220 °C) to a temperature below the UCST-type binodal temperature (lower than its melting point), liquid−liquid phase separation and melt-crystallization occurred simultaneously. Since phase separation precedes the crystallization process, the concentration of PVDF in the PVDF-rich phase is higher than that of PVDF in the single phase. Consequently, the rate of crystallization can be faster than when the crystallization occurs in a single phase. On the contrary, when crystallization precedes phase separation, the crystallization rate will be slower than when phase separation precedes crystallization.

Considering the application of an electric field to the blends during the temperature-quenching experiment from a single phase to a given temperature below the UCST, the rate of crystallization under an electric field is expected to be faster than in the absence of an electric field because the quench depth is larger due to the shift of the UCST to higher temperatures. To confirm this expectation, the H_v scattering intensity was measured with respect to time during temperature-quenching below the UCST for the PVDF/PMMA blends used in this study. The rate of crystallization can be evaluated using the invariant $Q_{H_v}(t)$ at time t because Q_{H_v} is only associated with optical anisotropic changes occurring in the course of crystallization (see eq 8) and not with phase separation. Since $Q_{H_v}(t)$ also varies with the sample thickness, we used the ratio of the invariant $Q_{H_v}(t)$ at time t and the invariant Q_{H_v} at the end, $Q_{H_v,end}$, to compare the relative rate of crystallization. Figures 10 and 11 show the normalized degree of crystallinity ($Q_{H_v}(t)/Q_{H_v,end}$) versus crystallization time for the 80/20 and 70/30 PVDF/PMMA blends, respectively, with and without an electric field of 7 MV/m after quenching from 220 °C to various temperatures below the

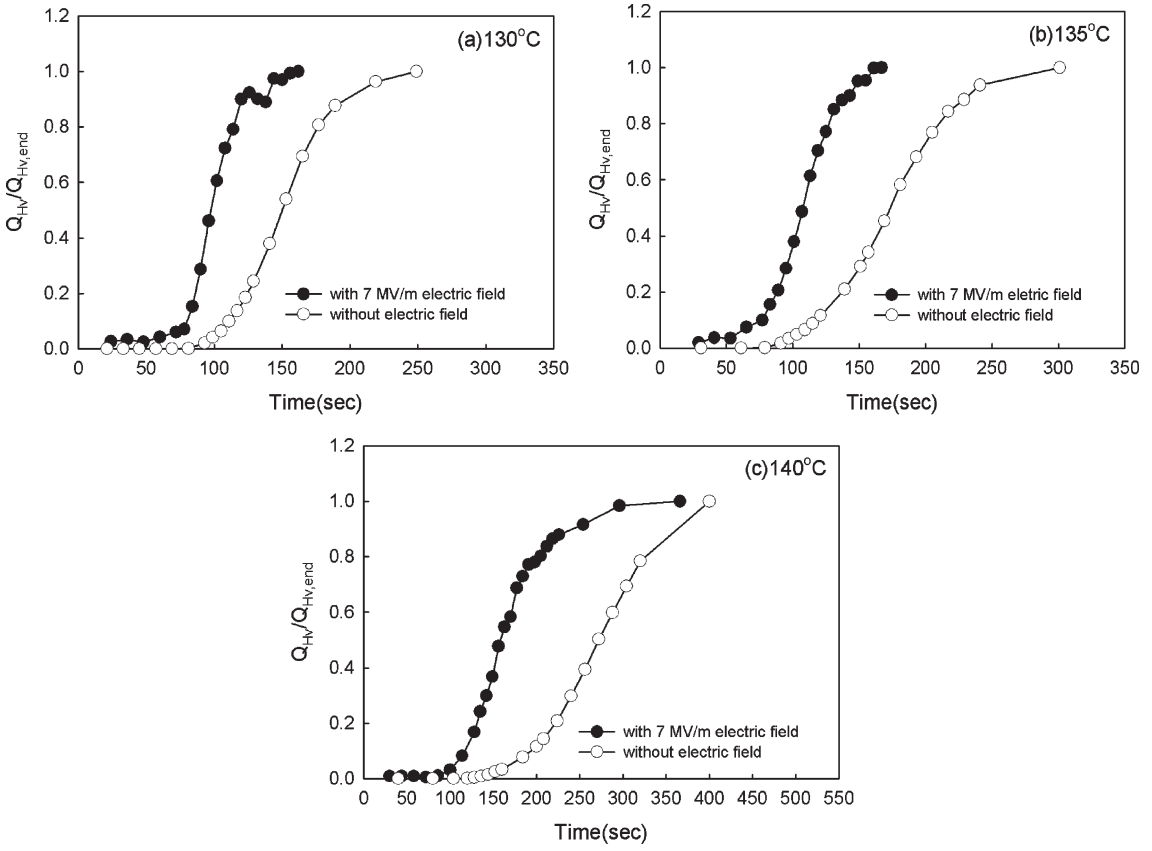

Figure 11. Normalized degree of crystallization versus time for the 70/30 PVDF/PMMA blend with and without an electric field of 7 MV/m after quenching from 220 °C to (a) 130 °C, (b) 135 °C, and (c) 140 °C below the UCST.

UCST. It was found that the crystallization rate under an electric field was faster than in the absence of an electric field for all the cases. Thus, under an electric field, the UCST shifts to higher temperatures and the rate of melt-crystallization increases in a single phase state.

V. Conclusions

The effect of electric field on phase separation behavior and crystallization kinetics in PVDF/PMMA blends can be summarized as follows:

UCST-type phase separation was empirically observed in PVDF/PMMA blends using time-resolved 2-D laser light scattering capable of measuring simultaneous H_v and V_v modes in the presence or absence of an electric field. An electric field strength of 7 MV/m shifted the UCST of the PVDF/PMMA blends to higher temperatures by 2−2.5 °C.

In the temperature range above the UCST (150 °C ≤ T ≤ 158 °C) where nonpolar α-crystals are dominantly formed, an electric field reduced the overall crystallization rate in neat PVDF and, in contrast, increased the crystallization rate in the PVDF/PMMA blends. γ-Crystals are formed at a lower crystallization temperature under the influence of increasing electric field strength than in the absence of an electric field. This is due to the faster nucleation rate of γ-crystals under an electric field. γ′-Crystals transformed from α-crystals were formed with increasing PMMA content and at higher crystallization temperatures.

When the polymer blends were quenched from a single phase state (at 220 °C) to a temperature below the UCST, which is lower than the melting point, liquid−liquid phase separation and melt-crystallization occur simultaneously. The rate of melt-crystallization below the UCST with an electric field is also faster than without an electric field due to an increase in quench depth caused by the shift of the UCST to a higher temperature.

Overall, the results obtained in this work are quite useful for understanding the effect of an electric field on the phase separation and crystallization behavior of PVDF/PMMA blends, and the experimental observations were in fairly good agreement with the trends predicted from our theoretical calculations.

Acknowledgment. This study was supported by the Korea Science and Engineering Foundation (KOSEF Grant R01-2000-00339) and Korea Science and Engineering Foundation (KOSEF) through the SRC/ERC Program of MOST/KOSEF (R11-2005-065).

References and Notes

(1) Olabisi, O.; Robeson, L. M.; Shaw, M. T. *Polymer-Polymer Miscibility*; Academic Press: New York, 1979.
(2) Reich, S.; Gordon, J. M. *J. Polym. Sci., Polym. Phys. Ed.* **1979**, *17*, 371–378.
(3) Kumaki, J.; Hashimoto, T. *Macromolecules* **1986**, *19*, 763–768.
(4) Kyu, T.; Saldanha, J. M. *Macromolecules* **1988**, *21*, 1021−1026, and references therein.
(5) Kyu, T.; Lim, D. S. *Macromolecules* **1991**, *24*, 3645–3650.
(6) Reister, E.; Muller, M.; Kumar, S. K. *Macromolecules* **2005**, *38*, 5158–5169.
(7) Wachowicz, M.; White, j. L. *Macromolecules* **2007**, *40*, 5433–5440.
(8) Nishi, T.; Wang, T. T. *Macromolecules* **1975**, *8*, 909–915.
(9) Tomura, H.; Saito, H.; Inoue, T. *Macromolecules* **1992**, *25*, 1611−1614, and references therein.
(10) Chen, H. L.; Li, L. J.; Lin, T. L. *Macromolecules* **1998**, *31*, 2255–2264.
(11) Wang, J.; Cheung, M. K.; Mi, Y. *Polymer* **2002**, *43*, 1357–1364.
(12) Walker, T. A.; Melnichenko, Y. B.; Wignall, G. D.; Spontak, R. J. *Macromolecules* **2003**, *36*, 4245−4249, and references therein.
(13) Matkar, R. A.; Kyu, T. *J. Phys. Chem. B* **2006**, *110*, 12728–12732.
(14) Rathi, P.; Huang, T. M.; Dayal, P.; Kyu, T. *J. Phys. Chem. B* **2008**, *112*, 6460–6466.

(15) Serpico, J. M.; Wnek, G. E.; Krause, S.; Smith, T. W.; Luca, D. J.; Laeken, A. V. *Macromolecules* **1991**, *24*, 6879–6881.
(16) Wirtz, D.; Berend, K.; Fuller, G. G. *Macromolecules* **1992**, *25*, 7234–7246.
(17) Gurovich, E. *Macromolecules* **1994**, *27*, 7339–7362.
(18) Gurovich, E. *Macromolecules* **1995**, *28*, 6078–6083.
(19) Hori, H.; Urakawa, O.; Yano, O.; Miyata, Q. T. C. *Macromolecules* **2007**, *40*, 389–394.
(20) Lee, J. S.; Prabu, A. A.; Kim, K. J.; Park, C. *Macromolecules* **2008**, *41*, 3598–3604.
(21) Glover, F. A.; Goulden, J. D. S. *Nature* (*London*) **1963**, *200*, 1165–1166.
(22) Koningsveld, R.; Kleintjens, L. A.; Shultz, A. R. *J. Polym. Sci., Polym. Phys.* **1970**, *8*, 1261–1278.
(23) Koberstein, J.; Russell, T. P.; Stein, R. S. *J. Polym. Sci., Polym. Phys.* **1979**, *17*, 1719–1730.
(24) Wallner, G. M.; Major, Z.; Maier, G. A.; Lang, R. W. *Polym. Test.* **2008**, *27*, 392–402.
(25) Marand, H. L.; Stein, R. S.; Stack, G. M. *J. Polym. Sci., Polym. Phys.* **1988**, *26*, 1361–1383.
(26) Marand, H. L.; Stein, R. S. *J. Polym. Sci., Polym. Phys.* **1989**, *27*, 1089–1106.
(27) Lee, J. S.; Cho, H. W.; Kim, K. J. *J. Korean Fiber Soc.* **2004**, *41*, 1–9.
(28) Okabe, Y.; Kyu, T.; Saito, H.; Inoue, T. *Macromolecules* **1998**, *31*, 5823–5829.
(29) Okabe, Y.; Kyu, T. *Polymer* **2004**, *45*, 8485–8490.
(30) Lee, J. S.; Kim, K. J. *Fibers Polym.* **2007**, *4*, 335–346.